

Published in final edited form as:

Biochemistry. 2010 June 29; 49(25): 5377–5389. doi:10.1021/bi100538b.

The Role of Lys-12 in Catalysis by Triosephosphate Isomerase: A Two-Part Substrate Approach[‡]

Maybelle K. Go, Astrid Koudelka, Tina L. Amyes, and John P. Richard*

Department of Chemistry, University at Buffalo, SUNY, Buffalo, New York 14260-3000

Abstract

We report that the K12G mutation at triosephosphate isomerase (TIM) from *Saccharomyces cerevisiae* results in: (1) A ca. 50-fold increase in K_m for the substrate glyceraldehyde 3-phosphate (GAP) and a 60-fold increase in K_i for competitive inhibition by the intermediate analog 2-phosphoglycolate, resulting from the loss of stabilizing ground state interactions between the alkylammonium side chain of Lys-12 and the ligand phosphodianion group. (2) A 12,000-fold decrease in k_{cat} for isomerization of GAP, suggesting a tightening of interactions between the side chain of Lys-12 and the substrate on proceeding from the Michaelis complex to the transition state. (3) A 6×10^5 -fold decrease in k_{cat}/K_m , corresponding to a total 7.8 kcal/mol stabilization of the transition state by the cationic side chain of Lys-12. The yields of the four products of the K12G TIM-catalyzed isomerization of GAP in D₂O were quantified as: dihydroxyacetone phosphate (DHAP), 27%; [1(*R*)-²H]-DHAP, 23%; [2(*R*)-²H]-GAP, 31%; and 18% methylglyoxal from an *enzyme-catalyzed* elimination reaction. The K12G mutation has only a small effect on the relative yields of the three products of proton transfer to the TIM-bound enediol(ate) intermediate in D₂O, but it strongly favors catalysis of the elimination reaction to give methylglyoxal. The K12G mutation also results in a ≥ 14 -fold decrease in k_{cat}/K_m for *isomerization* of bound glycolaldehyde (GA), although the dominant observed product of the mutant enzyme-catalyzed reaction of [1-¹³C]-GA in D₂O is [1-¹³C, 2,2-di-²H]-GA from a nonspecific *protein-catalyzed* reaction. The observation that the K12G mutation results in a large decrease in k_{cat}/K_m for the reactions of both GAP and the neutral truncated substrate [1-¹³C]-GA provides evidence for a stabilizing interaction between the cationic side chain of Lys-12 and negative charge that develops at the enolate-like oxygen in the transition state for deprotonation of the sugar substrate "piece".

Triosephosphate isomerase (TIM) ¹ catalyzes the stereospecific, reversible, 1,2-hydrogen shift at dihydroxyacetone phosphate (DHAP) to give (*R*)-glyceraldehyde 3-phosphate (GAP) by a single-base (Glu-165) proton transfer mechanism through an enzyme-bound *cis*-enediol(ate) intermediate (Scheme 1) (1,2). The enzyme's low molecular weight (dimer, 26 kDa/subunit), high cellular abundance (3), and the centrality of proton transfer at carbon in metabolic processes (4–6) have made TIM a prominent target for studies on the mechanism of enzyme action (1,7–10).

[‡]This work was supported by Grant GM39754 from the National Institutes of Health

*Author to whom correspondence should be addressed, Tel: (716) 645 4232, Fax: (716) 645 6963, jrichard@buffalo.edu.

¹Abbreviations: TIM, triosephosphate isomerase; DHAP, dihydroxyacetone phosphate; GAP, (*R*)-glyceraldehyde 3-phosphate; PGA, 2-phosphoglycolate; GA, glycolaldehyde; GPDH, glycerol 3-phosphate dehydrogenase; BSA, bovine serum albumin; MES, 2-(*N*-morpholino)ethanesulfonic acid; CAPSO, 3-(cyclohexylamino)-2-hydroxy-1-propanesulfonic acid; NADH, nicotinamide adenine dinucleotide, reduced form; TEA, triethanolamine; MOPS, 3-(*N*-morpholino)propanesulfonic acid; *Pfu*, DNA polymerase from the hyperthermophilic *Pyrococcus furiosus*; PCR, polymerase chain reaction; *DpnI*, restriction endonuclease from *Diplococcus pneumoniae* G41; NMR, nuclear magnetic resonance; D,L-GAP, D,L-glyceraldehyde 3-phosphate; *d*-DHAP, [1(*R*)-²H]-dihydroxyacetone phosphate; *d*-GAP, [2(*R*)-²H]-glyceraldehyde 3-phosphate; MG, methylglyoxal; PGH, 2-phosphoglycolohydroxamate;

Deprotonation of the truncated neutral substrate (*R*)-glyceraldehyde by TIM is ca. 10^9 -fold slower than the partly diffusion-controlled (11) turnover of the natural phosphorylated substrate GAP (12). We showed previously that more than 80% of the 4×10^{10} -fold enzymatic rate acceleration for carbon deprotonation of GAP is derived from the 12 kcal/mol "intrinsic phosphate binding energy" (13) of the small nonreacting phosphodianion group of the substrate (12,14). Similar intrinsic phosphate binding energies of 12 kcal/mol are observed for the decarboxylation reaction catalyzed by orotidine 5'-monophosphate decarboxylase (15) and the hydride transfer reaction catalyzed by glycerol 3-phosphate dehydrogenase (16).

We want to understand the source of the large 12 kcal/mol intrinsic phosphate binding energy for TIM. X-ray crystallographic analyses of TIM complexed with DHAP (7) or 2-phosphoglycolate (PGA) (10,17) reveal interactions between the ligand phosphodianion group 6 and the backbone amide NH groups of Ser-211 in loop 7, Gly-232 and Gly-233 in loop 8, and of Gly-171 in the flexible "phosphate gripper" loop 6 (18).² There should be little or no *enthalpic* advantage to stabilization of a TIM-bound ligand by hydrogen bonds between backbone amide NH groups and the ligand phosphodianion group, relative to its stabilization in aqueous solution by hydrogen bonding to water (19,20). However, there is probably a significant *entropic* advantage to formation of a network of four effectively *intramolecular* hydrogen bonds to a TIM-bound ligand relative to formation of four *intermolecular* hydrogen bonds in aqueous solution, because the latter is accompanied by the loss in translational and rotational entropy of four water molecules (19,20). Furthermore, hydrogen bonding to the backbone amide NH groups of Gly-232 and Gly-233 may be enhanced because these residues lie at the N-terminal end of a short α -helix that has its positive dipole directed toward the substrate phosphodianion group (18). We note however that it is difficult to examine by experiment the contribution of individual hydrogen bonds between substrate and backbone amide NH groups to the rate acceleration for TIM.

A major source of the intrinsic phosphate binding energy for TIM is the interaction between the substrate phosphodianion and the cationic alkylammonium side chain of Lys-12. The K12M mutant of yeast TIM was prepared in earlier work, but the effect of the mutation on the kinetic parameters could not be determined because the observed activity was due to contaminating wildtype TIM (21). This wildtype contaminant was presumed (21) to form as a result of rare errors in translation of the methionine codon (AUG) to give the product of translation of the closely related lysine codon (AAG). The observation of respectable activities for both the K12R and K12H mutants of yeast TIM, along with a distinctive pH-rate profile for 7 the K12H mutant, showed that a positively charged side chain at position 12 of TIM is required for the observation of robust enzymatic activity (21).

Electrostatic potential maps calculated from X-ray crystallographic data showed that the surface of the active site pocket for wildtype yeast TIM is cationic, while the corresponding surface for the K12M mutant is almost entirely anionic (22). These maps provided evidence that the cationic side chain of Lys-12 stabilizes the enzyme bound substrate phosphodianion. However, it is not clear whether this interaction is expressed entirely at the Michaelis complex (K_m effect) or if it strengthens on proceeding to the transition state for deprotonation of bound substrate (k_{cat} effect). We therefore aimed to characterize and quantify the effect of removal of the cationic side chain of Lys-12 on the activity of TIM, by substituting glycine for lysine at position 12. We have constructed the K12G mutant of yeast TIM by changing the native AAA lysine codon at position 12 to GGC coding for glycine. This substitution effectively eliminates the possibility of contamination by wildtype enzyme.

²Unless noted otherwise, residues are numbered according to the sequence for the enzyme from yeast.

We report here the preparation of K12G mutant yeast TIM and determination of the effect of this mutation on both the kinetic parameters and the product distribution for the turnover of the natural substrate GAP and of the truncated neutral substrate [1-¹³C]-glycolaldehyde ([1-¹³C]-GA). A comparison of the kinetic parameters for the wildtype and K12G TIM-catalyzed reactions of GAP shows that the alkylammonium side chain of Lys-12 stabilizes the transition state for isomerization of GAP by 7.8 kcal/mol. Around 30% of this interaction is expressed at the Michaelis complex with GAP, but ca. 70% (5.6 kcal/mol) is expressed specifically at the transition state for deprotonation of GAP (k_{cat} effect). We also observe a sizeable effect of the K12G mutation on the kinetic parameters for isomerization of the truncated substrate [1-¹³C]-GA to give [2-¹³C]-GA, which provides strong evidence for a stabilizing interaction between the cationic side chain of Lys-12 and negative charge that develops at the enolate-like oxygen in the transition state for deprotonation of this sugar substrate "piece".

MATERIALS AND METHODS

Materials

Glycerol 3-phosphate dehydrogenase from rabbit muscle (GPDH) and glycylglycine were from United States Biochemical. Bovine serum albumin (BSA) was from Roche. D,L-Glyceraldehyde 3-phosphate diethyl acetal (barium salt), dihydroxyacetone phosphate (lithium salt), 2-(N-morpholino)ethanesulfonic acid (MES), 3-(cyclohexylamino)-2-hydroxy-1-propanesulfonic acid (CAPSO), NADH (disodium salt) and Dowex 50WX4-200R were from Sigma. Triethanolamine hydrochloride (TEA.HCl) and imidazole were from Aldrich. 3-(N-Morpholino)propanesulfonic acid (MOPS) and ethylamine hydrochloride were from Fluka. Sodium phosphite (dibasic, pentahydrate) was from Riedel-de Haën (Fluka). [1-¹³C]-Glycolaldehyde (99% enriched with ¹³C at C-1, 0.09 M in water) was from Omicron Biochemicals. Deuterium oxide (99.9% D) and deuterium chloride (35% w/w, 99.9% D) were from Cambridge Isotope Laboratories. DEAE Sepharose (fast flow) was from GE Healthcare. Water was obtained from a Milli-Q Academic purification system. Imidazole was recrystallized from benzene. All other commercially available chemicals were reagent grade or better and were used without further purification.

2-Phosphoglycolic acid was prepared according to a literature procedure (23). The barium salt of D-glyceraldehyde 3-phosphate diethyl acetal was prepared by Dr. James Tait according to a literature procedure (24).

Preparation of Wildtype and K12G Mutant Yeast TIM

The plasmid containing the gene for wildtype TIM from *Saccharomyces cerevisiae* (25) and *Escherichia coli* strain DF502 (strep^R, tpi⁻, and his⁻) whose DNA lacks the gene for TIM (26) were generous gifts from Professor Nicole Sampson.

Site-directed mutagenesis of yeast TIM to introduce the K12G mutation was carried out using *Pfu* Ultra High Fidelity DNA polymerase following the Stratagene protocol. The starting plasmid DNA (30 ng) was placed into a PCR reaction mixture containing 5 μ L of 10x *Pfu* ultra buffer, 125 ng each of the forward and reverse mutagenesis primers, 5 μ L of a 2 mM dNTP mixture and 2.5 units of *Pfu* Ultra High Fidelity DNA polymerase in a final volume of 50 μ L. The parameters for the PCR were: 45 s at 95 °C followed by 17 cycles of 45 s at 95 °C, 1.5 min at 55 °C and 10 min at 68 °C. The primer used to introduce the K12G mutation, in which the altered codon is underlined, was:

5'-CT-TTC-TTT-GTC-GGT-GGT-AAC-TTT-GGC-TTA-AAC-GGT-TCC-AAA-CAA-TCC-3'

After completion of the PCR reaction, 30 units of *DpnI* were added to 30 μL of the reaction mixture followed by incubation for 1 h at 37 $^{\circ}\text{C}$, in order to degrade the methylated template DNA. *E. coli* strain K802 was transformed with 1 μL of the *DpnI* digested PCR product. Several colonies containing possible mutants were picked and the plasmid DNA was purified using the QIAprep Miniprep Kit from Qiagen. The presence of the gene for K12G mutant TIM was verified by sequencing at the Roswell Park Cancer Institute (Buffalo, NY).

E. coli strain DF502 was transformed with the plasmid containing the gene for wildtype or K12G mutant yeast TIM and the proteins were expressed and purified according to published procedures, with ion exchange chromatography performed using DEAE Sepharose (27,28). The purity of the protein in the individual column fractions was determined by gel electrophoresis. Fractions containing the desired TIM at better than ca. 95% purity were pooled and dialyzed against 20 mM TEA (pH 7.5).

Preparation of Solutions

Solution pH or pD was determined at 25 $^{\circ}\text{C}$ using an Orion model 720A pH meter equipped with a Radiometer pH4006-9 combination electrode that was standardized at pH 7.00 and 4.00 or 10.00 at 25 $^{\circ}\text{C}$. Values of pD were obtained by adding 0.40 to the observed reading of the pH meter (29).

[1- ^{13}C]-Glycolaldehyde (1 mL of a 90 mM solution in H_2O) was reduced to a volume of ca. 100 μL by rotary evaporation. 5 mL of D_2O was added and the volume was again reduced to ca. 100 μL by rotary evaporation. This procedure was repeated twice more and 900 μL of D_2O was added to the final solution to give a volume of ca. 1 mL. The stock solution of [1- ^{13}C]-GA in D_2O was stored at room temperature to minimize the content of glycolaldehyde dimer (30). The concentration of [1- ^{13}C]-GA in the stock solution was determined by ^1H NMR spectroscopy, as described previously (28,30,31).

Solutions of GAP in D_2O and of D,L-glyceraldehyde 3-phosphate (D,L-GAP) in H_2O were prepared by hydrolysis of the corresponding diethyl acetals, as described previously (28,32). The resulting solutions were stored at -20 $^{\circ}\text{C}$. These solutions were adjusted to the appropriate pD or pH using 1 M NaOD or 1 M NaOH before use, after which they were again stored at -20 $^{\circ}\text{C}$. The stock solution of PGA was prepared in D_2O and was adjusted to pD 6.9 with 1 M NaOD before use. The concentration of PGA in the stock solution was determined by ^1H NMR as follows: An aliquot (50 μL) of the stock solution of PGA was added to 700 μL of 30 mM imidazole buffer (pD 7.0, 20% free base). Comparison of the integrated areas of the signals due to the C-(4,5) protons of imidazole and the C-2 protons of PGA gave the concentration of PGA in the stock solution as 42 mM.

Buffered solutions of TEA, MES, MOPS, glycylglycine and carbonate in H_2O were prepared by neutralization of the acidic form with sufficient 1 M NaOH to give the desired pH. Buffered solutions of acetate and CAPSO in H_2O were prepared addition of sufficient 1 M HCl to the sodium salt to obtain the desired pH.

Before preparation of solutions in D_2O , the bulk of the water of crystallization of $\text{Na}_2\text{HPO}_3 \cdot 5\text{H}_2\text{O}$ was removed by drying *in vacuo* as described previously (30). The acidic protons of ethylamine hydrochloride were exchanged for deuterium by repeated dissolution in D_2O followed by removal of the solvent under reduced pressure and drying *in vacuo*. The stock solution of $\text{EtND}_3^+\text{Cl}^-$ in D_2O was adjusted to pD 6.7 using 1 M NaOD. Buffered solutions of imidazole and phosphite in D_2O were prepared by dissolving the basic form, and where appropriate NaCl, followed by the addition of a measured amount of a stock solution of DCl to give the desired buffer ratio.

Enzyme Assays

All enzyme assays were carried out at 25 °C. One unit is the amount of enzyme that converts 1 μmol of substrate to product in 1 min under the specified conditions. Changes in the concentration of NADH were calculated using an extinction coefficient of $6220 \text{ M}^{-1} \text{ cm}^{-1}$ at 340 nm. GPDH was dialyzed at 4 °C against 20 mM TEA (pH 7.5) and was assayed by monitoring the oxidation of NADH by DHAP at 340 nm, as described previously (28). Dilute solutions of TIM were stabilized by the inclusion of 0.01% (0.1 mg/mL) BSA. The subunit concentration of wildtype or K12G yeast TIM in stock solutions was determined from the absorbance at 280 nm using an extinction coefficient of $2.55 \times 10^4 \text{ M}^{-1} \text{ cm}^{-1}$ that was calculated using the ProtParam tool available on the ExPASy server (33,34). The concentration of GAP in stock solutions of GAP in D_2O or of D,L-GAP in H_2O was determined from the amount of NADH consumed during quantitative TIM-catalyzed isomerization of GAP to form DHAP that was coupled to the oxidation of NADH using GPDH.

The activities of wildtype and K12G mutant yeast TIM were determined by coupling the isomerization of GAP to form DHAP to the oxidation of NADH using GPDH (35). The standard assay mixture (1.0 mL) contained 30 mM TEA at pH 7.5, 0.2 mM NADH, 5 mM D,L-GAP (2.5 mM GAP) and ca. 1 unit of GPDH at $I = 0.10$ (NaCl). A low background velocity v_0 that is due mainly to the isomerization of GAP catalyzed by TIM that was present as an impurity in the commercial preparation of GPDH was determined over a period of 2 – 4 min. An aliquot of wildtype or K12G TIM was then added, and the total initial velocity v_{obsd} was determined by monitoring the reaction for an additional 5 – 10 min. The initial velocity of the TIM-catalyzed reaction was then calculated as $v_i = v_{\text{obsd}} - v_0$, where v_0 generally represented $\leq 2\%$ of v_{obsd} .

Values of K_i for competitive inhibition of wildtype and K12G mutant yeast TIM by PGA at pH 7.5 (30 mM TEA), 25 °C and $I = 0.10$ (NaCl) were determined using several concentrations of PGA up to 130 μM for wildtype or 2.1 mM for K12G mutant TIM.

pH-Rate Profile for Turnover of GAP by K12G TIM

The pH-dependence of k_{cat}/K_m for isomerization of GAP catalyzed by K12G mutant yeast TIM at 25 °C was determined using the 13 following buffers: pH 5.1, acetate; pH 5.6 and 6.3, MES; pH 7.1, MOPS; pH 7.5, TEA; pH 8.3, glycylglycine; pH 8.9, CAPSO; and pH 9.9, carbonate. The standard assay mixture (1.0 mL) contained 30 mM buffer, 0.2 mM NADH, 0.8 – 6 mM D,L-GAP (0.4 – 3 mM GAP) and ca. 1 unit of GPDH. The relative specific activity of the coupling enzyme GPDH was determined at each pH, and the amount used was adjusted so that the velocity of consumption of NADH was independent of the concentration of the coupling enzyme (35).

^1H NMR Analyses

^1H NMR spectra at 500 MHz were recorded in D_2O at 25 °C using a Varian Unity Inova 500 spectrometer that was shimmed to give a line width of ≤ 0.7 Hz for each peak of the doublet due to the C-1 proton of GAP hydrate, or ≤ 0.5 Hz for the downfield peaks of the double triplet due to the C-1 proton of $[1-^{13}\text{C}]$ -GA hydrate. Spectra (16 – 64 transients) were obtained using a sweep width of 6000 Hz, a pulse angle of 90° and an acquisition time of 4 – 6 s, with zero-filling of the data to 128 K. To ensure accurate integrals for the protons of interest, a relaxation delay between pulses of 120 s ($> 8T_1$) was used. Baselines were subjected to a first-order drift correction before determination of integrated peak areas. Chemical shifts are reported relative to HOD at 4.67 ppm.

K12G TIM-Catalyzed Reaction of GAP in D₂O Monitored by ¹H NMR

K12G TIM was exhaustively dialyzed at 4 °C against 10 mM imidazole (pD 7.9, 70% free base) in D₂O at $I = 0.10$ (NaCl). The reaction of GAP (10 mM) in the presence of K12G TIM in D₂O at pD 7.9 (10 mM imidazole), 25 °C and $I = 0.15$ (NaCl) was monitored by ¹H NMR spectroscopy, as described in earlier work (32). The fraction of the remaining substrate GAP (f_{GAP}) and the fraction of GAP converted to the products DHAP (f_{DHAP}), *d*-DHAP ($f_{\text{d-DHAP}}$), *d*-GAP ($f_{\text{d-GAP}}$) and methylglyoxal (MG, f_{MG}) at time t were determined from the integrated areas of the relevant ¹H NMR signals (normalized using the signal due to the C-(4,5) protons of imidazole as an internal standard), as described previously (32). A control experiment was carried out in order to monitor the rate of the nonenzymatic elimination reaction of GAP (10 mM) to give methylglyoxal (14) in D₂O at pD 7.9 (10 mM imidazole), 25 °C and $I = 0.15$ (NaCl).

K12G TIM-Catalyzed Reactions of [1-¹³C]-GA in D₂O Monitored by ¹H NMR

K12G TIM was exhaustively dialyzed at 4 °C against 30 mM imidazole (pD 7.0, 20% free base) in D₂O at $I = 0.10$ (NaCl) for reactions in the absence of phosphite and/or EtND₃⁺, or at $I = 0.024$ for reactions in their presence.

The K12G TIM-catalyzed reaction of [1-¹³C]-GA in D₂O at pD 7.0 (Reaction 1) was initiated by adding 650 μL of enzyme (ca. 13 mg/mL) to 350 μL of a solution containing [1-¹³C]-GA and NaCl to give final concentrations of 20 mM [1-¹³C]-GA, 20 mM imidazole and 240 μM K12G TIM in D₂O at pD 7.0 and $I = 0.10$ (NaCl). The K12G TIM-catalyzed reaction of [1-¹³C]-GA in D₂O at pD 7.0 in the presence of 100 mM EtND₃⁺ (Reaction 2) was initiated by adding 650 μL of enzyme (ca. 13 mg/mL) to 350 μL of a solution containing [1-¹³C]-GA and EtND₃⁺ to give final concentrations of 20 mM [1-¹³C]-GA, 20 mM imidazole, 100 mM EtND₃⁺ and 310 μM K12G TIM in D₂O at pD 7.0 and $I = 0.12$. The K12G TIM-catalyzed reaction of [1-¹³C]-GA in D₂O at pD 7.0 in the presence of 50 mM EtND₃⁺ and 10 mM phosphite dianion (20 mM total phosphite) (Reaction 3) was initiated by adding 600 μL of enzyme (ca. 9 mg/mL) to 250 μL of a solution containing [1-¹³C]-GA, phosphite buffer (50% free base) and EtND₃⁺ to give final concentrations of 20 mM [1-¹³C]-GA, 20 mM imidazole, 50 mM EtND₃⁺, 10 mM phosphite dianion (20 mM total phosphite) and 290 μM K12G TIM in D₂O at pD 7.0 and $I = 0.12$.

In each case, 750 μL of the reaction mixture was transferred to an NMR tube and ¹H NMR spectra (32 transients) at 25 °C were recorded over a period of 4 – 7 days. The remaining portion of the reaction mixture was incubated at 25 °C and the activity of K12G TIM was monitored by periodic standard assay (see above). For Reaction 1 there was a ca. 20% drop in the activity of K12G TIM during 78 h at 25 °C. For Reactions 2 and 3 there was a ca. 40% drop in the activity of K12G TIM during 7 days at 25 °C.

The fraction of the remaining substrate [1-¹³C]-GA, f_{S} , and the fraction of [1-¹³C]-GA converted to the identifiable products [1-¹³C, 2-²H]-GA and [1-¹³C, 2,2-di-²H₂]-GA were determined from the integrated areas of the relevant ¹H NMR signals (normalized using the signal due to the C-(4,5) protons of imidazole as an internal standard), as described previously (28).

Observed first-order rate constants, k_{obsd} , for the disappearance of [1-¹³C]-GA were determined from the slopes of linear semi-logarithmic plots of reaction progress against time according to eq 1. Observed second-order rate constants for the total *protein-catalyzed* reactions of [1-¹³C]-GA were calculated using eq 2, where $f_{\text{car}} = 0.061$ is the fraction of GA present in the reactive carbonyl form (30,31) and [E] is the concentration of K12G TIM.

$$\ln f_s = -k_{\text{obsd}}t \quad (1)$$

$$\left(\frac{k_{\text{cat}}}{K_m}\right)_{\text{obsd}} = \frac{k_{\text{obsd}}}{f_{\text{car}}[E]} \quad (2)$$

RESULTS

K12G TIM-Catalyzed Reaction of GAP in D₂O

The disappearance of the substrate and the appearance of the products of the nonenzymatic and K12G TIM-catalyzed reactions of GAP in D₂O was monitored by ¹H NMR spectroscopy, as described in previous work (32). Figure 1A shows the time course for the disappearance of GAP (10 mM) catalyzed by 85 μM K12G TIM in D₂O at pD 7.9 (10 mM imidazole), 25 °C and *I* = 0.15 (NaCl). The solid line shows the nonlinear least-squares fit of the experimental data to a single exponential which gave $k_{\text{obsd}} = 3.6 \times 10^{-4} \text{ s}^{-1}$ as the observed rate constant for disappearance of GAP (Table 1). Figure 1B shows the time dependence of the *observed* fractional yields of the four products of this reaction, $(f_p)_{\text{obsd}}$ (*P* = DHAP, *d*-DHAP, *d*-GAP or MG). These fractional yields were calculated from the fraction of the particular product *P* (see Materials and Methods) and the sum of the fractions of all the products of both the enzymatic and nonenzymatic reactions of GAP using eq 3 (Scheme 2). There is no significant change in $(f_p)_{\text{obsd}}$ for DHAP with time, but the changes with time in the observed fractional yields of *d*-DHAP (increasing) and *d*-GAP (decreasing) result from enzyme-catalyzed isomerization of *d*-GAP to give the thermodynamically favored product *d*-DHAP (32). Table 1 reports the *initial* fractional product yields, $(f_p)_o$ for DHAP, *d*-DHAP and *d*-GAP, or $(f_{\text{MG}})_{\text{tot}}$ for MG, that were determined by extrapolation of the observed product yields $(f_p)_{\text{obsd}}$ to zero time (intercepts in Figure 1B).

$$(f_p)_{\text{obsd}} = \frac{f_p}{f_{\text{DHAP}} + f_{\text{d-DHAP}} + f_{\text{d-GAP}} + f_{\text{MG}}} \quad (3)$$

$$(f_{\text{MG}})_N = \frac{k_N}{k_{\text{obsd}}} \quad (4)$$

$$(f_{\text{MG}})_E = (f_{\text{MG}})_{\text{tot}} - (f_{\text{MG}})_N \quad (5)$$

In a control experiment the nonenzymatic elimination reaction of GAP (10 mM) to form methylglyoxal (14) in D₂O at pD 7.9 (10 mM imidazole), 25 °C and *I* = 0.15 (NaCl) was monitored by ¹H NMR spectroscopy (32). The fit of the data to a single exponential gave the observed first-order rate constant for disappearance of GAP as $k_N = 1.7 \times 10^{-5} \text{ s}^{-1}$. This was combined with $k_{\text{obsd}} = 3.6 \times 10^{-4} \text{ s}^{-1}$ for the reaction of GAP in the presence of 85 μM K12G TIM, according to eq 4, to give the calculated fractional yield of methylglyoxal from the nonenzymatic elimination reaction in this experiment as $(f_{\text{MG}})_N = 0.05$ (Table 1). The total initial fractional yield of methylglyoxal $(f_{\text{MG}})_{\text{tot}} = 0.25$ (Table 1) is five-fold larger than $(f_{\text{MG}})_N$ because, unlike wildtype TIM, K12G TIM also catalyzes the elimination reaction of

GAP to give methylglyoxal. The initial fractional yield of methylglyoxal from the K12G TIM-catalyzed reaction ($f_{\text{MG}}^{\text{E}} = 0.20$ (Table 1) was calculated using eq 5.

K12G TIM-Catalyzed Reaction of [1-¹³C]-GA in D₂O

Figure 2 shows semi-logarithmic plots according to eq 1 of the time course for the disappearance of [1-¹³C]-GA in D₂O at pD 7.0 (20 mM imidazole) and 25 °C, monitored by ¹H NMR spectroscopy (28), in the presence of K12G TIM, K12G TIM and 100 mM EtND₃⁺, or K12G TIM, 50 mM EtND₃⁺ and 10 mM phosphite dianion (20 mM total phosphite). Table 2 gives the observed-first order rate constants for these reactions that were calculated from the slopes of these linear correlations that covered 1 – 2 half-times.

Figure 3 shows portions of the ¹H NMR spectrum at 500 MHz of the reaction mixture obtained from the reaction of [1-¹³C]-GA for 78 h in the presence of 240 μM K12G TIM in D₂O at pD 7.0 and 25 °C. Under our reaction conditions glycolaldehyde exists as 93.9% hydrate and 6.1% free carbonyl form (30,31) and the following chemical shifts refer to the hydrates of the isotopomers shown in Chart 1. The signal due to the C-1 proton of [1-¹³C]-GA appears as a double triplet at 4.945 ppm (¹J_{HC} = 163 Hz, ³J_{HH} = 5 Hz) (Figure 3B). The signal due to the C-1 proton of [1-¹³C, 2,2-di-²H]-GA appears as a broad doublet (¹J_{HC} = 163 Hz) at 4.930 ppm that is shifted 0.015 ppm upfield from the double triplet due to the C-1 proton of [1-¹³C]-GA as a result of the two β-deuteriums (Figure 3B). The signal due to the C-2 protons of [1-¹³C]-GA appears as a double doublet at 3.410 ppm (²J_{HC} = 3 Hz, ³J_{HH} = 5 Hz) (Figure 3A). The signals due to the C-2 protons of [2-¹³C]-GA and [1,2-di-¹³C]-GA, present initially at 0.8% and 0.9%, respectively, in our commercial [1-¹³C]-GA, appear at 3.410 ppm as a double doublet (¹J_{HC} = 142 Hz, ³J_{HH} = 5 Hz) and a double double doublet (¹J_{HC} = 142 Hz, ²J_{HC} = 3 Hz, ³J_{HH} = 5 Hz), respectively. Figure 3A (inset) shows the upfield peaks of these signals; the corresponding downfield peaks appear along with other small peaks for unidentified reaction products.

We observe that the major identifiable product of the reaction of [1-¹³C]-GA in the presence of K12G mutant TIM in D₂O is the doubly deuteriated isotopomer [1-¹³C, 2,2-di-²H-GA] which is formed in a *nonspecific* reaction occurring outside the active site (28). The fractional yield of this product, $f_{\text{P}} = 0.56$ (Table 2), was calculated from the normalized peak area for its C-1 proton, A_{P} , and the *difference* in the normalized peak area for the C-1 proton of the substrate [1-¹³C]-GA at time zero, $(A_{\text{S}})_{\text{0}}$, and at time t , A_{S} , according to eq 6. The signal due to the C-2 proton of the product of isomerization with deuterium exchange, [2-¹³C, 2-²H]-GA, would appear as a double double triplet at 3.389 ppm (¹J_{HC} = 142 Hz, ³J_{HH} = 5 Hz, ²J_{HD} ≈ 2 Hz) shifted 0.021 ppm upfield of the double doublet due to the C-2 protons of [2-¹³C]-GA as a result of the α-deuterium (28). However, this signal was not observed in the spectrum shown in Figure 3A.

$$f_{\text{P}} = \frac{A_{\text{P}}}{(A_{\text{S}})_{\text{0}} - A_{\text{S}}} \quad (6)$$

During the reaction of [1-¹³C]-GA catalyzed by *wildtype* TIM in D₂O we observed that enzyme-catalyzed isomerization of the substrate results in an increase in the peak area of the signals due to [2-¹³C]-GA (28). By contrast, we observe here that the peak area of the signal due to the C-2 protons of [2-¹³C]-GA (initially present as 0.8% of total GA) *decreases* during the reaction of [1-¹³C]-GA for 78 h in the presence of 240 μM K12G mutant TIM in D₂O. However, during this time there is a small *increase* in the *ratio* of the peak areas of the signals due to the C-2 protons of [2-¹³C]-GA and [1-¹³C]-GA from 0.008 to 0.010, but *no change* in the *ratio* (0.009) of the peak areas of the signals due to the C-2 protons of [1,2-di-¹³C]-GA and [1-¹³C]-GA. These changes in *relative* peak areas are

consistent with essentially equal velocities of conversion of the three starting isotopomers to their corresponding C-2 doubly deuteriated analogs, for which there are no ^1H NMR signals in the C-2 region, along with a *very slow* enzyme-catalyzed isomerization of $[1-^{13}\text{C}]\text{-GA}$ to give $[2-^{13}\text{C}]\text{-GA}$. These data are consistent with conversion of $\leq 0.2\%$ of $[1-^{13}\text{C}]\text{-GA}$ to $[2-^{13}\text{C}]\text{-GA}$ that accompanies the much faster conversion of 20% of $[1-^{13}\text{C}]\text{-GA}$ to $[1-^{13}\text{C}, 2,2\text{-di-}^2\text{H}]\text{-GA}$ during this 78 hour reaction. Therefore, the fractional yield of $[2-^{13}\text{C}]\text{-GA}$ (≤ 0.006 , Table 2) from the K12G TIM-catalyzed isomerization of $[1-^{13}\text{C}]\text{-GA}$ is estimated to be at least 100-fold smaller than the fractional yield of $[1-^{13}\text{C}, 2,2\text{-di-}^2\text{H}]\text{-GA}$ (0.56).

Table 2 also gives the fractional yields of the identifiable products of the K12G TIM-catalyzed reactions of $[1-^{13}\text{C}]\text{-GA}$ in the presence of 100 mM EtND_3^+ or 50 mM EtND_3^+ and 10 mM phosphite dianion. These yields were calculated from the normalized peak areas of the signals due to these products using eq 6. In all cases, the sum of the fractional yields of the products of these slow reactions of $[1-^{13}\text{C}]\text{-GA}$ is well under 100% (28). No attempt was made to identify the other pathways for the slow reactions $[1-^{13}\text{C}]\text{-GA}$ in the presence of K12G TIM.

Kinetic Parameters and pH-Rate Profile for Isomerization of GAP by K12G TIM

Figure 4 shows the Michaelis-Menten plot for the isomerization of GAP catalyzed by K12G mutant yeast TIM at pH 7.5 (30 mM TEA), 25 °C and $I = 0.10$ (NaCl). The solid line shows the nonlinear least squares fit of these data to the Michaelis-Menten equation which gave $k_{\text{cat}} = 0.6 \pm 0.2 \text{ s}^{-1}$ and $K_{\text{m}} = 50 \pm 20 \text{ mM}$ (Table 3); the dashed line is the linear relationship for the case $[\text{GAP}] \ll K_{\text{m}}$. Table 3 also gives the much more reliable value of $k_{\text{cat}}/K_{\text{m}} = 12 \pm 0.4 \text{ M}^{-1} \text{ s}^{-1}$ that was determined as the slope of the linear correlation of the data at $[\text{GAP}] \leq 3 \text{ mM}$ (Figure 4, inset).

Figure 5 shows the dependence of apparent the second-order rate constant $(k_{\text{cat}}/K_{\text{m}})_{\text{app}}$ for K12G TIM-catalyzed isomerization of GAP (determined as the slopes of plots of $v_i/[\text{E}]$ against $[\text{GAP}]$) on the concentration of 2-phosphoglycolate (PGA) at pH 7.5, 25 °C and $I = 0.10$ (NaCl). The value of $K_i = 1.1 \text{ mM}$ (Table 3) was determined from the nonlinear least squares fit of these data to eq 7 with $k_{\text{cat}}/K_{\text{m}} = 12 \text{ M}^{-1} \text{ s}^{-1}$ in the absence of PGA.

$$(k_{\text{cat}}/K_{\text{m}})_{\text{app}} = \frac{k_{\text{cat}}/K_{\text{m}}}{1 + [\text{PGA}]/K_i} \quad (7)$$

Figure 6 shows pH-rate profiles of the observed second-order rate constants $(k_{\text{cat}}/K_{\text{m}})_{\text{obsd}}$ for the isomerization of GAP catalyzed by wildtype TIM from chicken muscle (data of Plaut & Knowles (35)) and by K12G mutant yeast TIM (data from this work). The literature data for wildtype TIM were fit to eq 8, derived for Scheme 3, using values of $(k_{\text{cat}}/K_{\text{m}})^* = 0$, $\text{p}K_{\text{SH}} = 6.0$ for ionization of the phosphodianion group of GAP and $\text{p}K_{\text{EH}} = 9.2$ for ionization of an essential residue at TIM (35). The solid and dashed lines through the data for K12G yeast TIM compare the fit obtained using $k_{\text{cat}}/K_{\text{m}} = 12 \text{ M}^{-1} \text{ s}^{-1}$ (Table 3), $\text{p}K_{\text{SH}} = 6.0$, $\text{p}K_{\text{EH}} = 9.2$ and $(k_{\text{cat}}/K_{\text{m}})^* = 0$ (solid line) with that using $(k_{\text{cat}}/K_{\text{m}})^* = 1.1 \text{ M}^{-1} \text{ s}^{-1}$ (dashed line) that was obtained from least-squares analysis that included $(k_{\text{cat}}/K_{\text{m}})^*$ as an additional parameter.

$$(k_{\text{cat}}/K_{\text{m}})_{\text{obsd}} = \left(\frac{[\text{H}^+]}{(K_{\text{EH}} + [\text{H}^+])(K_{\text{SH}} + [\text{H}^+])} \right) \left[\left(\frac{k_{\text{cat}}}{K_{\text{m}}} \right) K_{\text{SH}} + \left(\frac{k_{\text{cat}}}{K_{\text{m}}} \right)^* [\text{H}^+] \right] \quad (8)$$

DISCUSSION

The X-ray crystal structure of yeast TIM shows that the cationic side chain of Lys-12 runs along the enzyme surface (7). Closure of phosphate gripper loop 6 over the substrate sequesters the carbon acid fragment from interaction with solvent, but the tip of the substrate phosphodianion group lies at the protein surface where it forms a solvent-separated ion pair with the cationic side chain of Lys-12 (7). X-ray crystallographic analysis of K12M/G15A TIM crystallized in the presence of the enediol(ate) intermediate analog 2-phosphoglycolohydroxamate (PGH) revealed no bound ligand and showed that the structure of this enzyme was nearly identical to that of unliganded wildtype TIM (22). We therefore do not expect that the K12G mutation will result in a large change in protein structure, but it should leave a small water-filled cleft at the protein surface.

We report here a second-order rate constant of $k_{\text{cat}}/K_m = 12 \text{ M}^{-1} \text{ s}^{-1}$ for isomerization of GAP catalyzed by K12G mutant yeast TIM at pH 7.5, 25 °C and $I = 0.10$ (Table 3). In a previous study of the K12M mutant, the apparent value of $k_{\text{cat}}/K_m = 30 \text{ M}^{-1} \text{ s}^{-1}$ was attributed to the presence of ca. 0.0005% contaminating wildtype TIM in the mutant enzyme preparation (21). By comparison, the lowered affinity of K12G TIM for GAP and PGA determined here (Table 3) shows that the observed activity of the K12G mutant cannot be due to a contaminating wildtype TIM activity. Table 3 also reports the kinetic parameters for turnover of GAP by wildtype yeast TIM determined in this work, which are in good agreement with the earlier literature values (36).

In an earlier study of K12M TIM it was concluded that this mutant has a very weak affinity for phosphodianion ligands. The value of $K_i = 1.1 \text{ mM}$ determined here for inhibition of K12G TIM by PGA at pH 7.5 (Figure 5 and Table 3) shows that the K12G mutant forms a moderately stable complex with this inhibitor trianion. However, it is more difficult to evaluate the stability of the complex of K12G TIM with GAP. The slight curvature in the Michaelis-Menten plot of $v_i/[E]$ against [GAP] (Figure 4) is consistent with $K_m = 50 \pm 20 \text{ mM}$, but these data also show a reasonable fit to a linear equation. We note that: (1) If the K12G mutation results in a similar 60-fold increase in the dissociation constants for both PGA and GAP, then the value of K_m for GAP would be ca. 60 mM which is close to $K_m \approx 50 \text{ mM}$ obtained from the data in Figure 4 and; (2) The effect of the K12G mutation on the affinity of the enzyme for GAP should not be any larger than the effect on its affinity for PGA, because the additional negative charge at PGA will tend to strengthen, not weaken, the interaction of the ligand with the cationic side chain of Lys-12 at the wildtype enzyme. Therefore, we conclude that K12G TIM has a weak affinity for GAP with $K_m = 50 - 60 \text{ mM}$.

K12G TIM-Catalyzed Reaction of GAP in D₂O

We reported previously that the reaction of GAP catalyzed by wildtype rabbit or chicken muscle TIM in D₂O, monitored for 2 – 5 h (32), results in formation of the three products of the enzyme-catalyzed reaction along with substantial formation of methylglyoxal from the competing *nonenzymatic* elimination reaction (Scheme 2) (14). We observe here that the K12G mutation at yeast TIM results in a large increase in the velocity of formation of methylglyoxal over that predicted for the competing *nonenzymatic* elimination reaction (Table 1). This shows that K12G TIM also catalyzes the elimination reaction of GAP to give methylglyoxal (Scheme 4). Table 1 reports the normalized fractional yields f_E of the products of the *enzymatic* reaction of GAP catalyzed by 85 μM and 12 μM K12G TIM in D₂O at pD 7.9. These yields were calculated using eq 9, where $(f_{\text{MG}})_E$ is the fractional yield of methylglyoxal from the enzymatic reaction that was calculated from the total fractional yield of methylglyoxal $(f_{\text{MG}})_{\text{tot}}$ as described in the Results section.

$$f_E = \frac{(f_P)_O}{(f_{\text{DHAP}})_O + (f_{d\text{-DHAP}})_O + (f_{d\text{-GAP}})_O + (f_{\text{MG}})_E} \quad (9)$$

$$(f_E)_{\text{PT}} = \frac{(f_P)_O}{(f_{\text{DHAP}})_O + (f_{d\text{-DHAP}})_O + (f_{d\text{-GAP}})_O} \quad (10)$$

A rate constant ratio $k_{\text{PT}}/k_{\text{elim}} \approx 1 \times 10^6$ was estimated for partitioning of the enzyme-bound enediol(ate) phosphate intermediate of the wildtype TIM-catalyzed reaction between protonation at carbon and elimination of inorganic phosphate (37). This is much larger than $k_{\text{PT}}/k_{\text{elim}} = 6.5$ for partitioning of the same enediol(ate) phosphate between proton transfer at carbon and elimination of phosphate within a loose complex with a small tertiary ammonium cation in solution (14). These observations show that interactions with wildtype TIM strongly stabilize the bound enediol(ate) phosphate intermediate towards elimination of inorganic phosphate (37,38). The absence of the alkylammonium side chain of Lys-12 at K12G mutant yeast TIM results in a dramatic change in the ratio of the yields of the products of proton transfer and elimination (Scheme 4), from $k_{\text{PT}}/k_{\text{elim}} \approx 1 \times 10^6$ (37) to $0.81/0.18 = 4.5$ (Table 1). This dramatic change in the partitioning of the enediol(ate) phosphate intermediate shows that interaction of the cationic side chain of Lys-12 with the bound enediol(ate) phosphate strongly protects this species from elimination of inorganic phosphate. Good yields of methylglyoxal are also observed from the reactions of GAP and DHAP catalyzed by a loop deletion mutant of TIM (38), because interactions between the enediol(ate) phosphate and the flexible loop (loop 6) of TIM play a vital role in preventing breakdown of the intermediate with loss of inorganic phosphate.

Table 1 also reports the normalized fractional yields $(f_E)_{\text{PT}}$ of the three products of *proton transfer* to the enzyme-bound enediol(ate) intermediate of the reactions of GAP catalyzed by wildtype TIM from rabbit or chicken muscle (32) and K12G mutant yeast TIM (this work, calculated using eq 10). These data show that the K12G mutation causes the yield of DHAP formed by intramolecular transfer of hydrogen from substrate GAP to decrease from 49% for the wildtype enzyme to 33% for the K12G mutant. There is good evidence that the H-labeled carboxylic acid side chain of Glu-165 at the TIM•enediol(ate) complex is sequestered from bulk solvent D₂O and that this residue undergoes exchange with a small pool of similarly sequestered hydrons followed by proton transfer to the enediol(ate) to form *d*-GAP and *d*-DHAP (Scheme 4) (39,40). Therefore, the decrease in the yield of the product of intramolecular transfer of hydrogen is *nominally* consistent with the conclusion that the K12G mutation increases the accessibility of the active site to the bulk solvent. The K12G mutation also results in an increase in the ratio of the yields of *d*-GAP and *d*-DHAP, from 0.7 for wildtype TIM to 1.3 for the K12G mutant. However, these small effects are difficult to rationalize in comparison with the very large 6×10^5 -fold effect of the K12G mutation on $k_{\text{cat}}/K_{\text{m}}$ for isomerization of GAP (Table 3).

We conclude that Lys-12 plays an important role in stabilizing both the transition state for deprotonation of GAP and of the bound enediol(ate) intermediate towards elimination of phosphate dianion. However, it plays a much less important role in controlling the partitioning of the enediol(ate) intermediate in D₂O between formation of DHAP, *d*-GAP and *d*-DHAP.

K12G TIM-Catalyzed Reaction of [1-¹³C]-GA in D₂O

The large difference between $k_{\text{cat}}/K_{\text{m}}$ for isomerization of GAP ($1.0 \times 10^8 \text{ M}^{-1} \text{ s}^{-1}$)³ and for deprotonation of glycolaldehyde (ca. $0.10 \text{ M}^{-1} \text{ s}^{-1}$)⁴ by wildtype chicken muscle TIM shows that interactions between the substrate phosphodianion and TIM provide a ca. 12 kcal/mol stabilization (intrinsic phosphate binding energy) of the transition state for proton transfer from GAP (12,16). Truncation of GAP to give the neutral substrate glycolaldehyde eliminates transition state stabilization resulting from interactions with the phosphodianion group. Therefore, the observation of a large effect of the K12G mutation on the rate constant for deprotonation of glycolaldehyde would provide direct evidence for stabilizing interactions between the excised cationic side chain of Lys-12 and the carbon acid substrate piece. This two-part substrate approach was used to probe the interactions of amino acid side chains with the phosphodianion and nucleoside portions of the substrate in the decarboxylation of orotidine 5'-monophosphate catalyzed by orotidine 5'-monophosphate decarboxylase (41).

We reported previously that the reaction of [1-¹³C]-GA catalyzed by wildtype chicken muscle TIM gives a ca. 50% combined yield of the isomerization product [2-¹³C]-GA, the product of isomerization with deuterium exchange [2-¹³C, 2-²H]-GA, and the product of deuterium exchange [1-¹³C, 2-²H]-GA resulting from the "specific" reactions of [1-¹³C]-GA at the enzyme active site (28) (Scheme 5). By contrast, the only clearly detectable product of the reaction of [1-¹³C]-GA catalyzed by K12G mutant yeast TIM is the dideuteriated isotopomer [1-¹³C, 2,2-di-²H]-GA which is formed in ca. 56% yield (Table 2). This isotopomer was also observed as a minor product (ca. 20% yield) of the wildtype chicken muscle TIM-catalyzed reaction where it was proposed to form by a "nonspecific" protein-catalyzed reaction that occurs outside the enzyme active site (28).

The second-order rate constant for the *nonspecific* K12G TIM-catalyzed reaction of [1-¹³C]-GA to give [1-¹³C, 2,2-di-²H]-GA that occurs outside the active site can be calculated as $k_{\text{cat}}/K_{\text{m}} = (0.11 \text{ M}^{-1} \text{ s}^{-1})(0.56) = 0.062 \text{ M}^{-1} \text{ s}^{-1}$, where $0.11 \text{ M}^{-1} \text{ s}^{-1}$ is the *observed* second-order rate constant for the K12G TIM-catalyzed disappearance of [1-¹³C]-GA and 0.56 is the fractional yield of [1-¹³C, 2,2-di-²H]-GA (Table 2). This rate constant is at least 90-fold larger than $(k_{\text{cat}}/K_{\text{m}})_{\text{iso}} \leq 7 \times 10^{-4} \text{ M}^{-1} \text{ s}^{-1}$ for isomerization of [1-¹³C]-GA *at the active site* to give [2-¹³C]-GA (Table 2). The corresponding second-order rate constant for isomerization of [1-¹³C]-GA catalyzed by wildtype chicken muscle TIM can be calculated from data in our previous work as $(k_{\text{cat}}/K_{\text{m}})_{\text{iso}} = 9.5 \times 10^{-3} \text{ M}^{-1} \text{ s}^{-1}$ (28).⁵ Therefore the K12G mutation results in at least a 14-fold decrease in $(k_{\text{cat}}/K_{\text{m}})_{\text{iso}}$ for isomerization of [1-¹³C]-GA. This provides *direct* evidence that the cationic side chain of Lys-12 stabilizes the transition state for proton transfer from glycolaldehyde by interaction with the carbon acid substrate piece. It is reasonable to conclude that this side chain also acts similarly to stabilize the transition state for isomerization of GAP by interaction with both the nonreacting phosphodianion *and* the reacting carbon acid fragments of the whole substrate.

Phosphite dianion strongly activates wildtype rabbit and chicken muscle TIM towards the isomerization of glycolaldehyde (28,30) and we have also found that alkylammonium cations strongly activate K12G mutant yeast TIM towards the isomerization of GAP (42). We therefore examined the K12G TIM-catalyzed reaction of [1-¹³C]-GA in D₂O in the

³Values of $k_{\text{cat}} = 2300 \text{ s}^{-1}$ and $K_{\text{m}} = 0.45 \text{ mM}$ for isomerization of GAP by chicken muscle TIM at pH 7.5 and 25 °C were reported in our earlier work (Ref. 28). GAP exists as 95% hydrate and 5% free carbonyl (the reactive form) in D₂O at pD 7.9, 25 °C and $I = 0.10$ (NaCl) (Ref. 32).

⁴Calculated using $(k_{\text{cat}}/K_{\text{m}})_{\text{obsd}} = 0.19 \text{ M}^{-1} \text{ s}^{-1}$ for enzyme-catalyzed disappearance of glycolaldehyde and the observation that 50% of the products of this reaction result from deprotonation of glycolaldehyde within the active site (Ref. 28).

⁵Calculated using $(k_{\text{cat}}/K_{\text{m}})_{\text{obsd}} = 0.19 \text{ M}^{-1} \text{ s}^{-1}$ for enzyme-catalyzed disappearance of glycolaldehyde and the observation that the isomerization product [2-¹³C]-GA is formed in a yield of 5% (Ref. 28).

presence of 100 mM EtND₃⁺ or 50 mM EtND₃⁺ and 10 mM phosphite dianion (Table 2). These reagents result in small increases in the observed second-order rate constant ($k_{\text{cat}}/K_{\text{m}})_{\text{obsd}}$ for the disappearance of [1-¹³C]-GA (Table 2). However, these increases do not result from catalysis of isomerization at the enzyme active site because there is no detectable formation of the isomerization product [2-¹³C]-GA (Table 2). No attempt was made to characterize the additional products of these slow reactions because the products do not appear to be formed at the active site of TIM. We conclude the following: (1) Interactions between the phosphite dianion activator and the cationic side chain of Lys-12 are essential for the observation of phosphite activation of the TIM-catalyzed deprotonation of GA (30). (2) Interactions between the phosphodianion group of GAP and exogenous ammonium cations are essential for the observation of rescue of the activity of K12G mutant TIM by these cations (42). However, K12G mutant TIM shows no detectable activity for isomerization of [1-¹³C]-GA in the presence of EtND₃⁺ and phosphite dianion, presumably because these ions show a weak affinity for binding to the mutant enzyme.

pH-Rate Profile for Isomerization of GAP by K12G Mutant Yeast TIM

Figure 6 shows the pH-rate profiles for $k_{\text{cat}}/K_{\text{m}}$ for isomerization of GAP catalyzed by wildtype chicken muscle TIM (data from the literature (35)) and K12G mutant yeast TIM (data from this work). The solid lines show the fits of the data to eq 8 with $(k_{\text{cat}}/K_{\text{m}})^* = 0$. The dashed line for K12G TIM shows that the inclusion of $(k_{\text{cat}}/K_{\text{m}})^* = 1.1 \text{ M}^{-1} \text{ s}^{-1}$ for turnover of GAP monoanion results in a small improvement in the fit of the experimental data to eq 8 (see Results section). This suggests that K12G TIM exhibits only a ca. 10-fold selectivity for catalysis of the isomerization of GAP dianion [$(k_{\text{cat}}/K_{\text{m}}) = 12 \text{ M}^{-1} \text{ s}^{-1}$, Table 3] over GAP monoanion [$(k_{\text{cat}}/K_{\text{m}})^* = 1.1 \text{ M}^{-1} \text{ s}^{-1}$].

The downward break centered at pH 9.2 for wildtype TIM cannot be due to deprotonation of the cationic side chain of Lys-12 because the same break is observed in the profile for K12G TIM (Figure 6).⁶ This demonstrates that $\text{p}K_{\text{a}} > 9.2$ for the cationic side chain of Lys-12, which is consistent with the salt bridge with the carboxylate side chain of Glu-97 observed at TIM•PGA and TIM•PGH complexes (10,17,43). It also suggests that there is a large distance between the side chains of Lys-12 and this second critical residue.

Specificity in Transition State Binding

The K12G mutation at yeast TIM results in a 5.5×10^5 -fold decrease in $k_{\text{cat}}/K_{\text{m}}$ for isomerization of GAP (Table 3), corresponding to a 7.8 kcal/mol stabilization of the transition state by the cationic side chain of Lys-12. This effect can be partitioned into a ca. 50-fold effect on K_{m} ($\Delta\Delta G = 2.3 \text{ kcal/mol}$) and a much larger ca. 12,000-fold effect on k_{cat} for isomerization of bound substrate ($\Delta\Delta G^{\ddagger} = 5.6 \text{ kcal/mol}$, Table 3). The effect of the mutation on K_{m} can be directly attributed to the loss of ground state electrostatic interactions between the substrate phosphodianion group and the cationic side chain of Lys-12. More importantly, the large effect on k_{cat} shows that there is a significant *strengthening* of the interactions between the ligand and the alkylammonium side chain of Lys-12 on moving from the ground state Michaelis complex to the transition state for carbon deprotonation. The most striking structural change on moving from the Michaelis complex to the *enediol(ate)-like* transition state for deprotonation of GAP is the change in formal charge at the substrate carbonyl oxygen, from 0 to -1, and the change in the total charge at bound ligand, from -2 to -3. This increase in negative charge is expected to result in an increase in the stabilizing electrostatic interactions between with the alkylammonium side chain of Lys-12 and the altered substrate in the transition state (44).

⁶The similarity of the kinetic parameters for wildtype TIM from chicken muscle (Ref. 35) and from yeast (Table 3 and Ref. 36) at pH 7.5 suggests that the appearance of the pH-rate profiles for these enzymes should also be similar.

The K12G mutation also results causes in at least a 14-fold decrease in $(k_{\text{cat}}/K_{\text{m}})_{\text{iso}}$ for *isomerization* of bound glycolaldehyde (*vide infra*), which shows that the cationic side chain of Lys-12 acts to stabilize the transition state for a proton transfer from a neutral substrate piece that lacks a phosphodianion group. This provides evidence for a significant stabilizing interaction between the cationic side chain of Lys-12 and the developing negative charge on the sugar substrate piece in an enediol(ate)-like transition state. It is in accord with computational studies that pointed to the dominant role of Lys-12 in stabilization of the transition state for formation of an enediolate intermediate by carbon deprotonation of the whole substrate DHAP or GAP (44,45).

The role of Lys-12 in catalysis of isomerization has also been inferred from an inspection of the X-ray crystal structure of yeast TIM complexed with DHAP (Figure 7) (7). The alkylammonium side chain of Lys-12 lies roughly equidistant from the phosphodianion and carbonyl groups of bound DHAP and is expected to interact with both centers. This side chain likely does not form a hydrogen bond with the phosphate dianion in the ground state Michaelis complex because the X-ray crystal structure reveals the presence of a water molecule between the cationic side chain of Lys-12 and the phosphodianion group of DHAP, which attenuates the electrostatic interaction (Figure 7) (7). This interaction might be strengthened by a shift in the position of the water to allow for closer proximity of the interacting charges at the transition state for proton transfer. However, we have no evidence to support this proposal and we note that a bridging water molecule in this position is also observed at complexes between TIM and the intermediate analogs PGH (43) and PGA (10).

The stretching frequency for the C-2 carbonyl group of DHAP bound to the H95Q and H95N mutants of yeast TIM lies between 1732 and 1742 cm^{-1} (46), which is similar to the carbonyl stretching frequency of 1732 cm^{-1} for DHAP in water (47). This suggests that there is no additional polarization of the carbonyl π -bond of enzyme-bound DHAP due to a hydrogen-bonding interaction with Lys-12 (21). Although there is no crystal structure for the complex between TIM and GAP, the large effect of the K12G mutation on k_{cat} for isomerization of GAP (Table 3) provides strong evidence that the cationic side chain of Lys-12 stabilizes negative charge that develops at O-1 at the transition state for deprotonation of GAP.

Charged Enediolate or Neutral Enediol Intermediate?

Studies of the nonenzymatic deprotonation of GAP in water show that direct Brønsted base-catalyzed deprotonation of the substrate to form a negatively charged enediolate intermediate is favored energetically over any competing Brønsted acid-catalyzed pathway to form the enediol (14). This is because the enolate oxygen of the enediolate intermediate is relatively weakly basic ($\text{p}K_{\text{a}} \approx 11$ for the enol (14,48)), so that there is no significant advantage to concerted catalysis by relatively weak Brønsted acids (49). Brønsted general acid catalysis of the deprotonation of enzyme-bound GAP to form an enediol intermediate would be favored if proton transfer from the enzyme to the enediolate were strongly favorable (50).

We suggest that there is a strong catalytic imperative to the avoidance of full proton transfer to the enediolate oxyanion and which dictates the use of a neutral imidazole side chain of His-95 (25), rather than the more acidic imidazolium cation, as the catalytic electrophile at TIM. Full proton transfer to the enediolate oxyanion would eliminate the large stabilizing electrostatic interaction with the cationic side chain of Lys-12. However, partial proton transfer from the neutral imidazole of His-95 to the oxyanion allows for effective transition state stabilization by hydrogen bonding (46), while at the same time maintaining the critical stabilizing electrostatic interaction with the cationic side chain of Lys-12.

It is not obvious that enolate anions, whose formation from neutral molecules is intrinsically more difficult in solvents of low dielectric constant than in water, should in fact be formed *more easily* at the nonpolar active sites of protein catalysts (51–55) than in aqueous solution. However, zwitterions are strongly stabilized by their transfer from aqueous solution to organic solvents (56–58), and the formation of the effectively intramolecular (59,60) ion pairs between enzyme catalysts and immobilized bound substrates will be favored entropically over the bimolecular formation of ion pairs between small molecules in solution. Others have noted that enzyme active sites provide a highly organized environment for chemical reactions (51,61,62), where appropriately placed amino acid side chains act to stabilize bound ions of opposite charge.

REFERENCES

1. Knowles JR, Albery WJ. Perfection in enzyme catalysis: the energetics of triosephosphate isomerase. *Acc. Chem. Res.* 1977; 10:105–111.
2. Rieder SV, Rose IA. Mechanism of the triose phosphate isomerase reaction. *J. Biol. Chem.* 1959; 234:1007–1010. [PubMed: 13654309]
3. Shonk CE, Boxer GE. Enzyme patterns in human tissues. I. Methods for the determination of glycolytic enzymes. *Cancer Res.* 1964; 24:709–721. [PubMed: 14188477]
4. Gerlt JA, Gassman PG. Understanding the rates of certain enzyme-catalyzed reactions: Proton abstraction from carbon acids, acyl transfer reactions, and displacement reactions of phosphodiester. *Biochemistry.* 1993; 32:11943–11952. [PubMed: 8218268]
5. Richard JP, Amyes TL. Proton transfer at carbon. *Cur. Opin. Chem. Biol.* 2001; 5:626–633.
6. Amyes, TL.; Richard, JP. Hynes, JT.; Klinman, JP.; Limbach, HH.; Schowen, RL. Hydrogen-Transfer Reactions, Volume 3, Biological Aspects I-II. Weinheim: Wiley-VCH; 2007. Proton Transfer to and from carbon in model systems; p. 949-973.
7. Jogl G, Rozovsky S, McDermott AE, Tong L. Optimal alignment for enzymatic proton transfer: structure of the Michaelis complex of triosephosphate isomerase at 1.2-Å resolution. *Proc. Natl. Acad. Sci. U. S. A.* 2003; 100:50–55. [PubMed: 12509510]
8. Xiang J, Sun J, Sampson NS. The importance of hinge sequence for loop function and catalytic activity in the reaction catalyzed by triosephosphate isomerase. *J. Mol. Biol.* 2001; 307:1103–1112. [PubMed: 11286559]
9. Xiang J, Jung J-y, Sampson NS. Entropy effects on protein hinges: The reaction catalyzed by triosephosphate isomerase. *Biochemistry.* 2004; 43:11436–11445. [PubMed: 15350130]
10. Kursula I, Wierenga RK. Crystal structure of triosephosphate isomerase complexed with 2-phosphoglycolate at 0.83-Å resolution. *J. Biol. Chem.* 2003; 278:9544–9551. [PubMed: 12522213]
11. Blacklow SC, Raines RT, Lim WA, Zamore PD, Knowles JR. Triosephosphate isomerase catalysis is diffusion controlled. *Biochemistry.* 1988; 27:1158–1165. [PubMed: 3365378]
12. Amyes TL, O'Donoghue AC, Richard JP. Contribution of phosphate intrinsic binding energy to the enzymatic rate acceleration for triosephosphate isomerase. *J. Am. Chem. Soc.* 2001; 123:11325–11326. [PubMed: 11697989]
13. Morrow JR, Amyes TL, Richard JP. Phosphate binding energy and catalysis by small and large molecules. *Acc. Chem. Res.* 2008; 41:539–548. [PubMed: 18293941]
14. Richard JP. Acid-base catalysis of the elimination and isomerization reactions of triose phosphates. *J. Am. Chem. Soc.* 1984; 106:4926–4936.
15. Amyes TL, Richard JP, Tait JJ. Activation of orotidine 5'-monophosphate decarboxylase by phosphite dianion: The whole substrate is the sum of two parts. *J. Am. Chem. Soc.* 2005; 127:15708–15709. [PubMed: 16277505]
16. Tsang W-Y, Amyes TL, Richard JP. A substrate in pieces: Allosteric activation of glycerol 3-phosphate dehydrogenase (NAD⁺) by phosphite dianion. *Biochemistry.* 2008; 47:4575–4582. [PubMed: 18376850]

17. Lolis E, Petsko GA. Crystallographic analysis of the complex between triosephosphate isomerase and 2-phosphoglycolate at 2.5-Å resolution: implications for catalysis. *Biochemistry*. 1990; 29:6619–6625. [PubMed: 2204418]
18. Knowles JR. To build an enzyme. *Philos. Trans. R. Soc. London, Ser. B*. 1991; 332:115–121. [PubMed: 1678530]
19. Klotz IM, Franzen JS. Hydrogen bonds between model peptide groups in solution. *J. Am. Chem. Soc.* 1962; 84:3461–3466.
20. Susi H, Timasheff SN, Ard JS. Near infrared investigation of interamide hydrogen bonding in aqueous solution. *J. Biol. Chem.* 1964; 239:3051–3054. [PubMed: 14217895]
21. Lodi PJ, Chang LC, Knowles JR, Komives EA. Triosephosphate isomerase requires a positively charged active site: The role of lysine-12. *Biochemistry*. 1994; 33:2809–2814. [PubMed: 8130193]
22. Joseph-McCarthy D, Lolis E, Komives EA, Petsko GA. Crystal structure of the K12M/G15A triosephosphate isomerase double mutant and electrostatic analysis of the active site. *Biochemistry*. 1994; 33:2815–2823. [PubMed: 8130194]
23. O'Connor EJ, Tomita Y, McDermott AE. Synthesis of (1,2-¹³C₂)-2-phosphoglycolic acid. *J. Labelled Compd. Radiopharm.* 1994; 34:735–740.
24. Bergemeyer, HU.; Haid, E.; Nelboeck-Hochstetter, M. Office, UP., editor. US: 1972.
25. Lodi PJ, Knowles JR. Neutral imidazole is the electrophile in the reaction catalyzed by triosephosphate isomerase: structural origins and catalytic implications. *Biochemistry*. 1991; 30:6948–6956. [PubMed: 2069953]
26. Straus D, Gilbert W. Chicken triosephosphate isomerase complements an *Escherichia coli* deficiency. *Proc. Natl. Acad. Sci. U. S. A.* 1985; 82:2014–2018. [PubMed: 3885220]
27. Sun J, Sampson NS. Understanding protein lids: kinetic analysis of active hinge mutants in triosephosphate isomerase. *Biochemistry*. 1999; 38:11474–11481. [PubMed: 10471299]
28. Go MK, Amyes TL, Richard JP. Hydron transfer catalyzed by triosephosphate isomerase. Products of the direct and phosphite-activated isomerization of [1-¹³C]-glycolaldehyde in D₂O. *Biochemistry*. 2009; 48:5769–5778. [PubMed: 19425580]
29. Glasoe PK, Long FA. Use of glass electrodes to measure acidities in deuterium oxide. *J. Phys. Chem.* 1960; 64:188–190.
30. Amyes TL, Richard JP. Enzymatic catalysis of proton transfer at carbon: activation of triosephosphate isomerase by phosphite dianion. *Biochemistry*. 2007; 46:5841–5854. [PubMed: 17444661]
31. Collins GCS, George WO. Nuclear magnetic resonance spectra of glycolaldehyde. *J. Chem. Soc. (B)*. 1971:1352–1355.
32. O'Donoghue AC, Amyes TL, Richard JP. Hydron transfer catalyzed by triosephosphate isomerase. Products of isomerization of (*R*)-glyceraldehyde 3-phosphate in D₂O. *Biochemistry*. 2005; 44:2610–2621. [PubMed: 15709774]
33. Gasteiger E, Gattiker A, Hoogland C, Ivanyi I, Appel RD, Bairoch A. ExPASy: The proteomics server for in-depth protein knowledge and analysis. *Nucleic Acids Res.* 2003; 31:3784–3788. [PubMed: 12824418]
34. Gasteiger, E.; Hoogland, C.; Gattiker, A.; Duvaud, S.; Wilkins, MR.; Appel, RD.; Bairoch, A. *Proteomics Protocols Handbook*. Walker, JM., editor. Totowa, NJ: Humana Press Inc; 2005. p. 571-607.
35. Plaut B, Knowles JR. pH-Dependence of the triose phosphate isomerase reaction. *Biochem. J.* 1972; 129:311–320. [PubMed: 4643319]
36. Nickbarg EB, Knowles JR. Triosephosphate isomerase: energetics of the reaction catalyzed by the yeast enzyme expressed in *Escherichia coli*. *Biochemistry*. 1988; 27:5939–5947. [PubMed: 3056516]
37. Richard JP. Kinetic-parameters for the elimination reaction catalyzed by triosephosphate isomerase and an estimation of the reactions physiological significance. *Biochemistry*. 1991; 30:4581–4585. [PubMed: 2021650]
38. Pompliano DL, Peyman A, Knowles JR. Stabilization of a reaction intermediate as a catalytic device: definition of the functional role of the flexible loop in triosephosphate isomerase. *Biochemistry*. 1990; 29:3186–3194. [PubMed: 2185832]

39. O'Donoghue AC, Amyes TL, Richard JP. Hydron transfer catalyzed by triosephosphate isomerase. Products of isomerization of dihydroxyacetone phosphate in D₂O. *Biochemistry*. 2005; 44:2622–2631. [PubMed: 15709775]
40. O'Donoghue AC, Amyes TL, Richard JP. Slow proton transfer from the hydrogen-labelled carboxylic acid side chain (Glu-165) of triosephosphate isomerase to imidazole buffer in D₂O. *Org. Biomol. Chem*. 2008; 6:391–396. [PubMed: 18175010]
41. Barnett SA, Amyes TL, Wood BM, Gerlt JA, Richard JP. Dissecting the Total Transition State Stabilization Provided by Amino Acid Side Chains at Orotidine 5'-Monophosphate Decarboxylase: A Two-Part Substrate Approach. *Biochemistry*. 2008; 47:7785–7787. [PubMed: 18598058]
42. Go, MK. Ph. D. Thesis. SUNY: University at Buffalo; 2009.
43. Davenport RC, Bash PA, Seaton BA, Karplus M, Petsko GA, Ringe D. Structure of the triosephosphate isomerase-phosphoglycolohydroxamate complex: an analog of the intermediate on the reaction pathway. *Biochemistry*. 1991; 30:5821–5826. [PubMed: 2043623]
44. Bash PA, Field MJ, Davenport RC, Petsko GA, Ringe D, Karplus M. Computer simulation and analysis of the reaction pathway of triosephosphate isomerase. *Biochemistry*. 1991; 30:5826–5832. [PubMed: 2043624]
45. Cui Q, Karplus M. Triosephosphate isomerase: A theoretical comparison of alternative pathways. *J. Am. Chem. Soc.* 2001; 123:2284–2290. [PubMed: 11456876]
46. Komives EA, Chang LC, Lolis E, Tilton RF, Petsko GA, Knowles JR. Electrophilic catalysis in triosephosphate isomerase: the role of histidine-95. *Biochemistry*. 1991; 30:3011–3019. [PubMed: 2007138]
47. Belasco JG, Knowles JR. Direct observation of substrate distortion by triosephosphate isomerase using Fourier transform infrared spectroscopy. *Biochemistry*. 1980; 19:472–477. [PubMed: 7356939]
48. Keeffe, JR.; Kresge, AJ. Kinetics and mechanism of enolization and ketonization. In: Rappoport, Z., editor. *The Chemistry of Enols*. Chichester: John Wiley and Sons; 1990. p. 399-480.
49. Jencks WP. Requirements for general acid-base catalysis of complex reactions. *J. Am. Chem. Soc.* 1972; 94:4731–4732.
50. Richard JP. The Enhancement of Enzymatic Rate Accelerations by Brønsted Acid-Base Catalysis. *Biochemistry*. 1998; 37:4305–4309. [PubMed: 9556344]
51. Sham YY, Muegge I, Warshel A. The effect of protein relaxation on charge-charge interactions and dielectric constants of proteins. *Biophys. J.* 1998; 74:1744–1753. [PubMed: 9545037]
52. Simonson T, Brooks CL. Charge Screening and the Dielectric Constant of Proteins: Insights for Molecular Dynamics. *J. Am. Chem. Soc.* 1996; 118:8452–8458.
53. Simonson T, Carlsson J, Case DA. Proton Binding to Proteins: pK_a Calculations with Explicit and Implicit Solvent Models. *J. Am. Chem. Soc.* 2004; 126:4167–4180. [PubMed: 15053606]
54. Antosiewicz J, McCammon JA, Gilson MK. The determinants of pK_as in proteins. *Biochemistry*. 1996; 35:7819–7833. [PubMed: 8672483]
55. Georgescu RE, Alexov EG, Gunner MR. Combining conformational flexibility and continuum electrostatics for calculating pK_as in proteins. *Biophys. J.* 2002; 83:1731–1748. [PubMed: 12324397]
56. Richard JP, Amyes TL. On the importance of being zwitterionic: enzymic catalysis of decarboxylation and deprotonation of cationic carbon. *Bioorg. Chem.* 2004; 32:354–366. [PubMed: 15381401]
57. Rios A, Amyes TL, Richard JP. Formation and stability of organic zwitterions in aqueous solution: enolates of the amino acid glycine and its derivatives. *J. Am. Chem. Soc.* 2000; 122:9373–9385.
58. Price WD, Jockusch RA, Williams ER. Binding energies of protonated betaine complexes: A probe of zwitterion structure in the gas phase. *J. Am. Chem. Soc.* 1998; 120:3474–3484. [PubMed: 16543945]
59. Jencks WP. Binding energy, specificity and enzymic catalysis: The Circe effect. *Adv. Enzymol. Relat. Areas Mol. Biol.* 1975; 43:219–410. [PubMed: 892]
60. Jencks WP. On the attribution and additivity of binding energies. *Proc. Natl. Acad. Sci. U. S. A.* 1981; 78:4046–4050. [PubMed: 16593049]

61. Warshel A. Electrostatic origin of the catalytic power of enzymes and the role of preorganized active sites. *J. Biol. Chem.* 1998; 273:27035–27038. [PubMed: 9765214]
62. Cannon WR, Benkovic SJ. Solvation, Reorganization Energy, and Biological Catalysis. *J. Biol. Chem.* 1998; 273:26257–26260. [PubMed: 9756847]

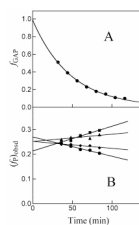


Figure 1.

Data for the reaction of GAP (10 mM) in the presence of 85 μ M K12G TIM in D₂O at pD 7.9 (10 mM imidazole), 25 °C and $I = 0.15$ (NaCl) monitored by ¹H NMR spectroscopy. **A.** Timecourse for the first-order disappearance of the substrate GAP. **B.** Dependence of the observed fractional yields of the products on time. Extrapolation of these data to zero time (solid lines) gave the initial fractional yields of the products of the enzyme-catalyzed and nonenzymatic reactions of GAP, $(f_P)_0$ or $(f_{MG})_{tot} = (f_{MG})_N + (f_{MG})_E$ reported in Table 1. (◆), Methylglyoxal; (■), *d*-DHAP; (▲), DHAP; (●), *d*-GAP.

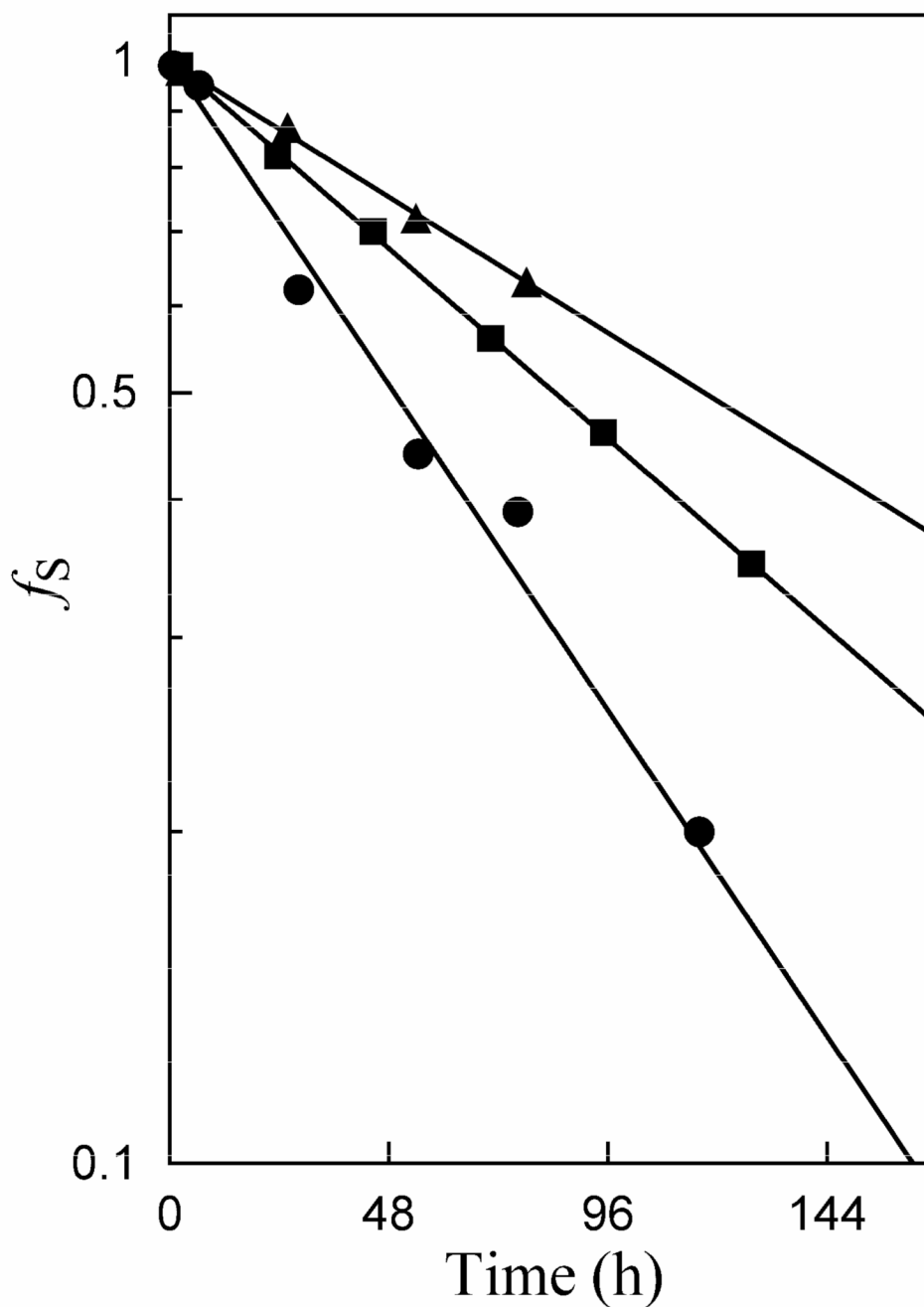


Figure 2. Semi-logarithmic plots of the fraction of remaining substrate against time for the reaction of [1-¹³C]-glycolaldehyde in the presence of K12G TIM in D₂O at pD 7.0 (20 mM imidazole) and 25 °C. The observed rate constants were determined from the slopes according to eq 1. (▲) 240 μM K12G TIM at $I = 0.10$; (■) 310 μM K12G TIM and 100 mM EtND₃⁺ at $I = 0.12$; (●) 290 μM K12G TIM, 50 mM EtND₃⁺ and 10 mM HPO₃²⁻ at $I = 0.12$.

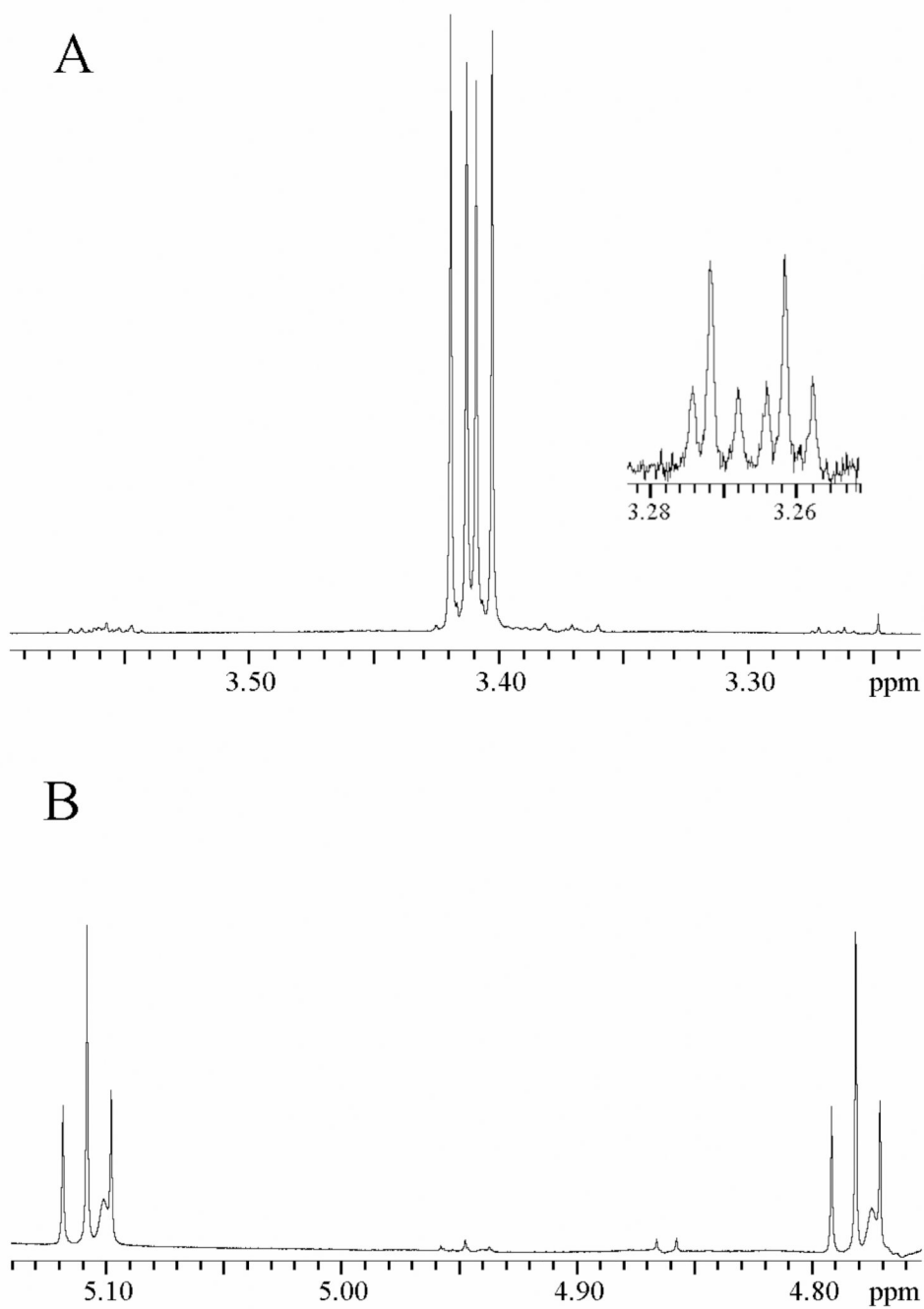


Figure 3. Portions of the ^1H NMR spectrum at 500 MHz of the reaction mixture obtained from the reaction of $[1\text{-}^{13}\text{C}]\text{-GA}$ (20 mM) for 78 h in the presence of $240\ \mu\text{M}$ K12G TIM in D_2O at pD 7.0, $25\ ^\circ\text{C}$ and $I = 0.10$ (NaCl). **A.** The spectrum in the region of the C-2 hydron(s) of the isotopomers of GA. **B.** The spectrum in the region of the C-1 hydron of the isotopomers of GA.

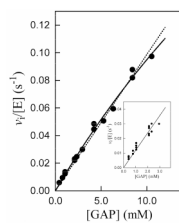


Figure 4. Michaelis-Menten plot of initial velocity data for the isomerization of GAP catalyzed by K12G TIM at pH 7.5 (30 mM TEA), 25 °C and $I = 0.10$ (NaCl). The solid line is the fit of the data to the Michaelis-Menten equation, and the dashed line is the linear relationship for the case $[GAP] \ll K_m$. The inset shows the linear correlation of the data for $[GAP] \leq 3$ mM, the slope of which gives $k_{cat}/K_m = 12 M^{-1} s^{-1}$.

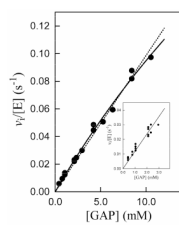


Figure 5.

The dependence of the apparent second-order rate constant $(k_{\text{cat}}/K_{\text{m}})_{\text{app}}$ for the isomerization of GAP catalyzed by K12G mutant yeast TIM on the concentration of 2-phosphoglycolate at pH 7.5 (30 mM TEA), 25 °C and $I = 0.10$ (NaCl).

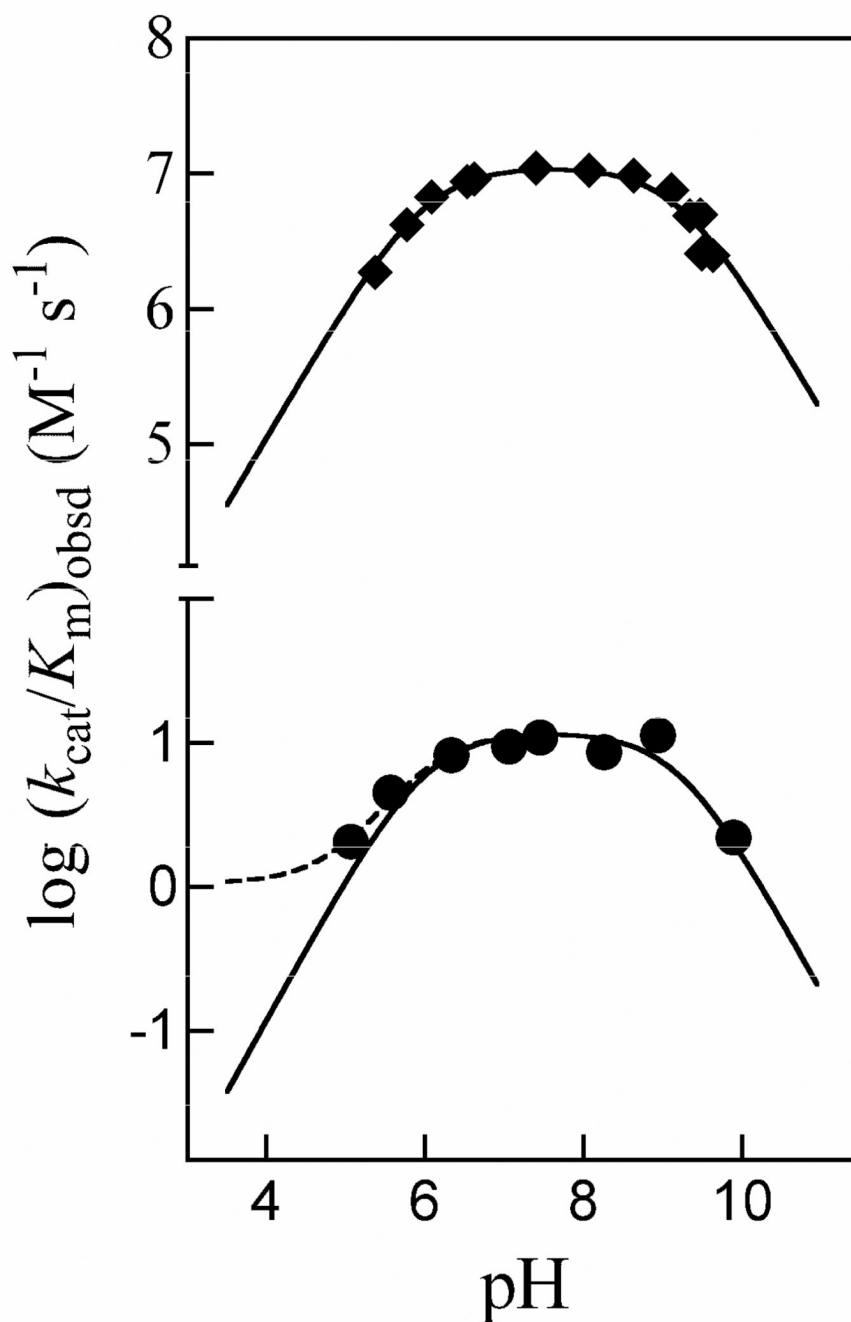


Figure 6.

The pH dependence of the observed second-order rate constant (k_{cat}/K_m)_{obsd} for the isomerization of GAP catalyzed by wildtype and K12G TIM. (◆) Data of Plaut & Knowles for wildtype TIM from chicken muscle at 30 °C (35). The solid line shows the fit of the data to eq 8 with $(k_{cat}/K_m)^* = 0$. (●) Data from this work for K12G mutant yeast TIM at 25 °C. The solid and dashed lines compare the nonlinear least squares fits of these data to eq 8 using values of $(k_{cat}/K_m)^* = 0$ and $1.1 \text{ M}^{-1} \text{ s}^{-1}$ for turnover of GAP monoanion, respectively (Scheme 3).

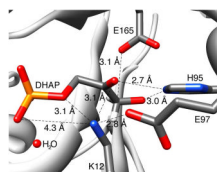
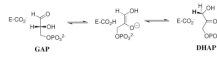
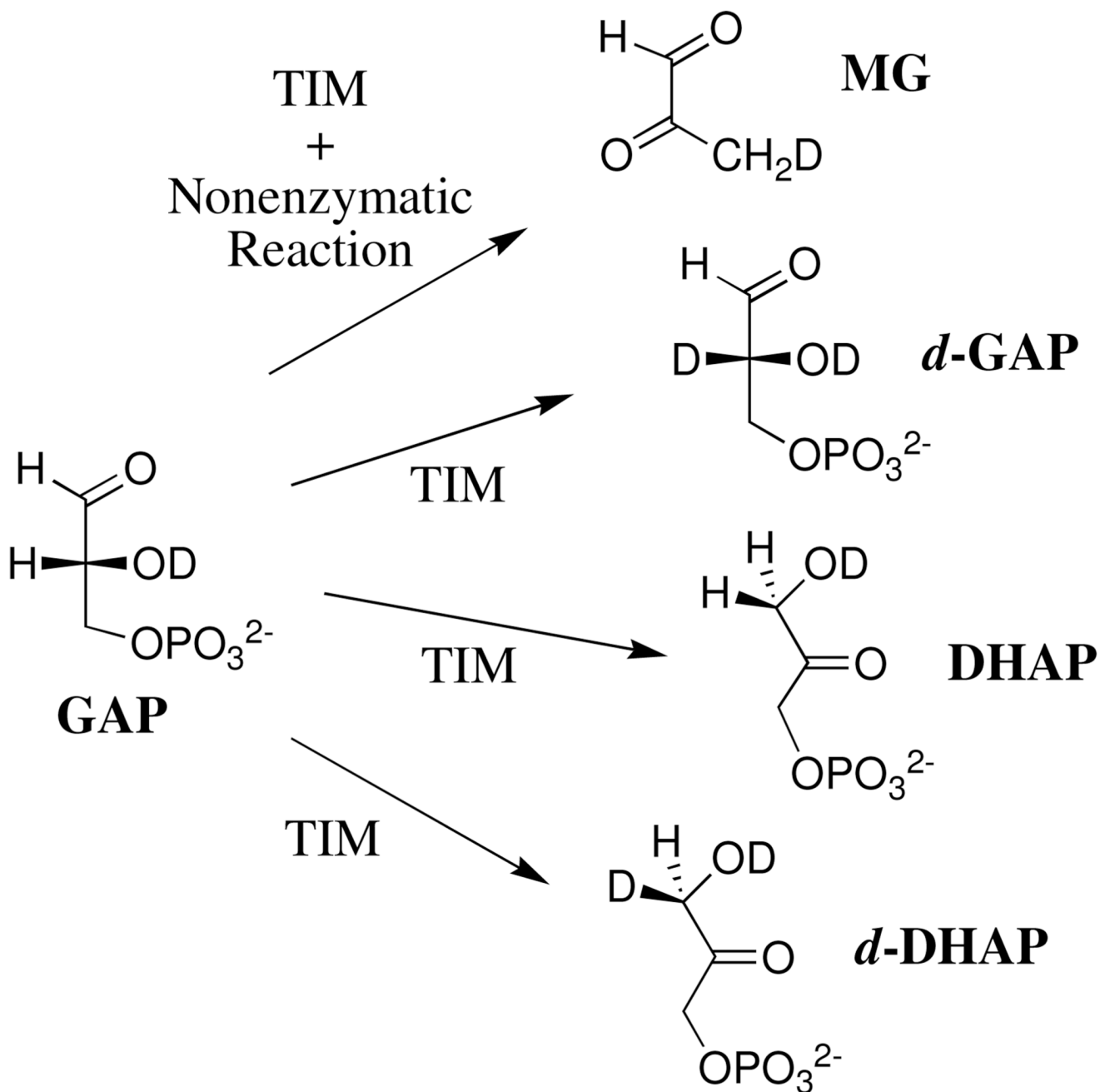
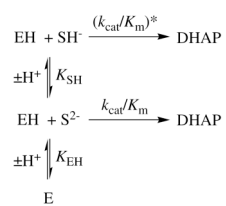


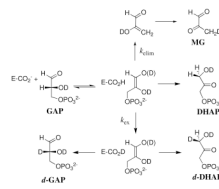
Figure 7. The structure of the active site of TIM, taken from the X-ray crystal structure of McDermott and coworkers (PDB entry 1NEY) (7), showing the distances between the ammonium nitrogen of Lys-12 and the functional groups of bound substrate DHAP.

**Scheme 1.**

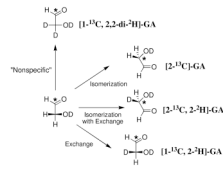


Scheme 2.

**Scheme 3.**



Scheme 4.

**Scheme 5.**

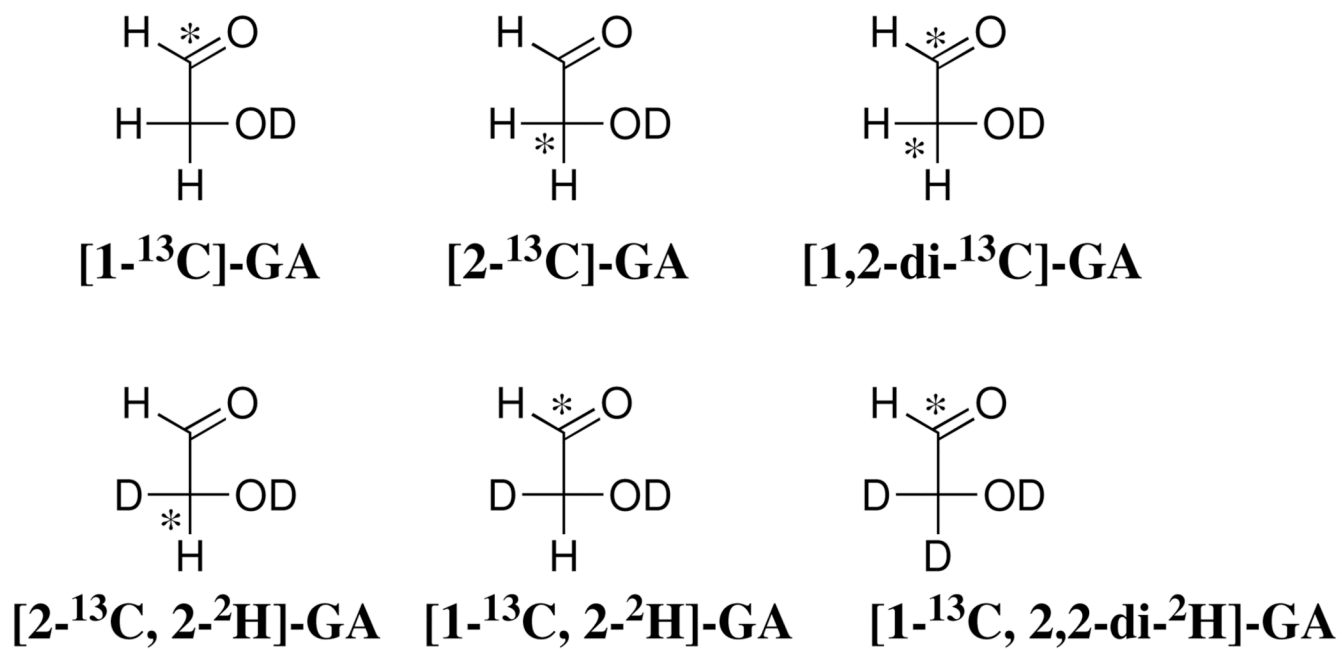


Chart 1.

Fractional Product Yields for the Reaction of (*R*)-Glyceraldehyde 3-Phosphate in the Presence of K12G Mutant Yeast Triosephosphate Isomerase in D₂O.^a

Table 1

[K12G TIM]	k_{obsd} (s ⁻¹) ^b	MG ($f_{\text{MG}}^{\text{tot}}$) ^c	MG (f_{MG}^{N}) ^d	MG (f_{MG}^{E}) ^e	<i>d</i> -GAP (f_{P}^{d}) ^f	DHAP (f_{P}^{d}) ^f	<i>d</i> -DHAP (f_{P}^{d}) ^f
85 μM	3.6×10^{-4}	0.25	0.05	0.20	0.27	0.25	0.21
					0.28	0.26	0.22
	f_{E}^{g}				0.35	0.33	0.28
	(f_{E}^{PT}) ^h						
12 μM	8.2×10^{-5}	0.34	0.21	0.13	0.26	0.22	0.19
				0.16	0.33	0.28	0.24
	f_{E}^{g}				0.40	0.33	0.29
	(f_{E}^{PT}) ^h						
Average Values		0.18 ± 0.02	0.31 ± 0.03	0.27 ± 0.01	0.23 ± 0.01		
	f_{E}^{g}				0.38	0.33	0.29
	(f_{E}^{PT}) ^h				(0.21) ⁱ	(0.49) ⁱ	(0.31) ⁱ

^aProduct distributions for the reaction of GAP (10 mM) at pD 7.9 (10 mM imidazole), 25 °C and $I = 0.15$ (NaCl) were determined by ¹H NMR spectroscopy as described previously (32)

^bObserved first-order rate constant for disappearance of GAP in the presence of the indicated concentration of K12G TIM.

^cTotal initial fractional yield of methylglyoxal determined by extrapolation of ($f_{\text{P}}^{\text{obsd}}$) to zero time (intercept in Figure 1B).

^dInitial fractional initial yield of methylglyoxal from the competing nonenzymatic reaction of GAP, calculated using eq 4.

^eInitial fractional yield of methylglyoxal from the enzymatic reaction of GAP, calculated using eq 5.

^fInitial fractional product yields determined by extrapolation of ($f_{\text{P}}^{\text{obsd}}$) to zero time (intercepts in Figure 1B).

^gNormalized fractional yields of the products of the *enzymatic* reaction of GAP, calculated using eq 9.

^hNormalized fractional yields of the three products of *proton transfer* to the enzyme-bound enediolate intermediate, calculated using eq 10.

ⁱData for the wildtype enzyme from chicken muscle taken from previous work (32).

Rate and Product Data for the Reactions of [1-¹³C]-GA in the Presence of K12G Mutant Yeast Triosephosphate Isomerase and the Potential Activators EtND₃⁺ and Phosphite Dianion in D₂O.^a

Table 2

[K12G TIM]	Activator	k_{obsd}^b (s ⁻¹)	$(k_{\text{cat}}/K_{\text{m}})_{\text{obsd}}^c$ (M ⁻¹ s ⁻¹)	$(k_{\text{cat}}/K_{\text{m}})_{\text{iso}}^d$ (M ⁻¹ s ⁻¹)	Fractional Product Yield			
					[2- ¹³ C]-GA	[1- ¹³ C, 2- ² H]-GA	[1- ¹³ C, 2,2-di- ² H]-GA	Total ^e
240 μM	None ^f	1.6×10^{-6}	0.11	$\leq 7 \times 10^{-4}$	≤ 0.006 g	small	0.56	0.56
310 μM	100 mM EtND ₃ ⁺ ^h	2.3×10^{-6}	0.12		none detected	0.10	0.20	0.30
290 μM	50 mM EtND ₃ ⁺ + 10 mM HPO ₃ ²⁻ ^h	3.8×10^{-6}	0.22		none detected	0.14	0.19	0.32

^aProduct distributions for the reaction of [1-¹³C]-GA (20 mM) at pD 7.0 (20 mM imidazole) and 25 °C were determined by ¹H NMR spectroscopy as described previously (28)

^bObserved first-order rate constant for the disappearance of [1-¹³C]-GA.

^cTotal observed second-order rate constant for the specific and nonspecific protein-catalyzed reactions.

^dSecond-order rate constant for the specific K12G TIM-catalyzed isomerization of [1-¹³C]-GA to give [2-¹³C]-GA, calculated as the product of $(k_{\text{cat}}/K_{\text{m}})_{\text{obsd}} = 0.11 \text{ M}^{-1} \text{ s}^{-1}$ and 0.006 as the upper limit on the fractional yield of [2-¹³C]-GA.

^eTotal fractional yield of the identifiable products.

^fAt I = 0.10 (NaCl).

^gUpper limit on the fractional yield of [2-¹³C]-GA, see text.

^hAt I = 0.12 (NaCl).

Table 3

Kinetic Parameters for Isomerization of GAP by Wildtype and K12G Mutant Yeast Triosephosphate Isomerase.^a

Yeast TIM	k_{cat}^b S ⁻¹	K_m^b mM	k_{cat}/K_m M ⁻¹ s ⁻¹	K_i for PGA mM
Wildtype	7300 ± 400	1.1 ± 0.2	6.6 × 10 ^{6c}	0.019 ± 0.004 ^d
K12G	0.6 ± 0.2	50 ± 20	12 ± 0.4 ^e	1.1 ± 0.2 ^f
Effect ^g	1.2 × 10 ⁴	50	5.5 × 10 ⁵	60
ΔΔG or ΔΔG [‡] kcal/mol	5.6	2.3	7.8	2.4

^a At pH 7.5 (30 mM TEA), 25 °C and $I = 0.10$ (NaCl). Quoted errors are standard errors obtained from least squares analysis.

^b Determined from the fit of initial velocity data to the Michaelis-Menten equation.

^c Calculated as the ratio of the values of k_{cat} and K_m

^d Determined by global nonlinear least squares analysis of initial velocity data in the presence of zero, 21 and 130 μM PGA.

^e Determined as the slope of the plot of $v_i/[E]$ against [GAP] for [GAP] ≤ 3 mM (Figure 4, inset).

^f Determined from the nonlinear least squares fit of the data in Figure 5 to eq 7.

^g The effect of the K12G mutation on the kinetic parameter.